Tetracyanomanganate(II) and Its Salts of Divalent First-Row Transition Metal Ions

Jamie L. Manson,[†] Wayne E. Buschmann,[‡] and Joel S. Miller*

Department of Chemistry, University of Utah, 315 South 1400 E. Rm. 2124, Salt Lake City, Utah 84112-0850

Received September 27, 2000

The first known paramagnetic, tetrahedral cyanide complex, $[Mn^{II}(CN)_4]^{2-}$, is formed by the photoinduced decomposition of $[Mn^{IV}(CN)_6]^{2-}$ in nonaqueous solutions or by thermal decomposition in the solid state. In acetonitrile or dichloromethane, photoexcitation into the ligand-to-metal charge transfer band (λ_{max} = 25 700 cm^{-1}, ϵ = 3700 cm^{-1} M^{-1}) causes the homolytic cleavage of cyanide radicals and reduction of Mn^{IV}. Free cyanide in dichloromethane leads to the isolation of polycyanide oligomers such as $[C_{12}N_{12}]^{2-}$ and $[C_4N_4]^-$, which was crystallographically characterized as the PPN^+ salt $C_{40}H_{30}N_5P_2$: monoclinic space group = $I2/a$, a = 18.6314(2) Å, b = 9.1926(1) Å, c = 20.8006(1), β =106.176(2)°, Z = 4]. In the solid state Mn^{IV}−CN bond homolysis is thermally activated above 122 °C, according to differential scanning calorimetry measurements, leading to the reductive elimination of cyanogen. The $[Mn^{II}(CN)_4]^{2-}$ ion has a dynamic solution behavior, as evidenced by its concentration-dependent electronic and electron paramagnetic spectra, that can be attributed to aggregation of the coordinatively and electronically unsaturated (four-coordinate, 13-electron) metal center. Due to dynamics and lability of $[Mn^{II}(CN)_4]^{2-}$ in solution, its reaction with divalent first-row transition metal cations leads to the formation of lattice compounds with both tetrahedral and square planar local coordination geometries of the metal ions and multiple structural and cyano-linkage isomers. α-$Mn^{II}[Mn^{II}(CN)_4]$ has an interpenetrating sphalerite- or diamond-like network structure with a unit cell parameter of a = 6.123 Å ($P\bar{4}3m$ space group) while a β-phase of this material has a noninterpenetrating disordered lattice containing tetrahedral $[Mn^{II}(CN)_4]^{2-}$. Linkage isomerization or cyanide abstraction during formation results in α-$Mn^{II}[Co^{II}(CN)_4]$ and $Mn^{II}[Ni^{II}(CN)_4]$ lattice compounds, both containing square planar tetracyanometalate centers. α-$Mn^{II}[Co^{II}(CN)_4]$ is irreversibly transformed to its β-phase in the solid state by heating to 135 °C, which causes a geometric isomerization of $[Co^{II}(CN)_4]^{2-}$ from square planar (ν_{CN} = 2114 cm^{-1}, S = $^1/_2$) to tetrahedral (ν_{CN} = 2158 cm^{-1}, S = $^3/_2$) as evidenced by infrared and magnetic susceptibility measurements. $Mn^{II}[Ni^{II}(CN)_4]$ is the only phase formed with Ni^{II} due to the high thermodynamic stability of square planar $[Ni^{II}(CN)_4]^{2-}$.

Introduction

Photochemical and thermal decomposition of homoleptic metal cyanide complexes is documented with several examples.[1−3] The photochemical processes fall into two general categories, photooxidation−reduction and photosubstitution reactions.[1] Photooxidation−reduction reactions are typically initiated by a ligand-to-metal charge transfer (LMCT) transition into an excited state that favors ligand−metal bond homolysis. Photosubstitution (e.g., aquation), in contrast, is typically initiated by ligand-field excited states. Thermolysis of cyanometalates in the solid state can result in loss of cyanide radicals in the form of cyanogen[3] accompanied by reduction of the metal center. This type of process has also been reported for $Li_2Mn^{IV}F_6$ in the solid state as a preparation of $Li_2Mn^{II}F_4$.[4]

Both photochemical[5] and thermal decomposition of $[Mn^{IV}(CN)_6]^{2-}$ lead to the formation of $[Mn^{II}(CN)_4]^{2-}$ (**1**),[6] the first member of a new class of paramagnetic, tetrahedral, and coordinatively unsaturated cyanometalates. This result is unusual since percyano complexes of the first-row transition metals are well-known to favor coordinatively saturated octahedral geometries.[2,7] Occasionally, however, there are deviations from this trend. Some well-characterized nonoctahedral examples include seven-coordinate $[V^{III}(CN)_7]^{4-}$ [7d] and the diamagnetic four-coordinate square planar-d^8 $[M^{II}(CN)_4]^{2-}$ (e.g., M = Ni, Pd, Pt) and tetrahedral-d^{10} (e.g., M = Zn^{II}, Cd^{II}, Hg^{II}) complexes.[2] The rare, d^7 low-spin, S = $^1/_2$, square planar $[Co^{II}(CN)_4]^{2-}$ attests to the strong ligand-field strength imposed by the cyanide ligand.[7b,c]

$[Mn^{II}(CN)_4]^{2-}$ elicits an interesting question regarding its ligand-field properties; since it is tetrahedral and consists of a strong ligand field, CN^-, is it high- or low-spin? All known homoleptic cyano complexes are low-spin;[2,7] however, virtually all known tetrahedral metal complexes are high-spin resulting from the decreased crystal field stabilization with respect to

[†] Present address: Chemistry and Materials Science Divisions, Argonne National Laboratory, 9700 S. Cass Ave., Argonne, IL 60439.

[‡] Present address: Bioscience Division, Los Alamos National Laboratory, Los Alamos, NM 87544.

(1) Balzani, V.; Carassiti, V. *Photochemistry of Coordination Compounds*; Academic Press: New York, 1970.

(2) (a) Sharpe, A. G. *The Chemistry of Cyano Complexes of the Transition Metals*; Academic Press: New York, 1976. (b) Shriver, D. F. *Struct. Bonding* **1966**, *1*, 33.

(3) (a) Buschmann, W. E.; Ensling, J.; Gütlich, P.; Miller, J. S. *Chem.—Eur. J.* **1999**, *5*, 3019. (b) Mohai, V. B. *Z. Anorg. Allg. Chem.* **1972**, *392*, 287. (c) Seifer, G. B.; Belova, V. I.; Makarova, Z. A. *Russ. J. Inorg. Chem. (Engl.)* **1964**, *9*, 844.

(4) (a) Wandner, K.-H.; Hoppe, R. *Z. Anorg. Allg. Chem.* **1988**, *557*, 153. (b) Wandner, K.-H.; Hoppe, R. *Z. Anorg. Allg. Chem.* **1987**, *546*, 113.

(5) Buschmann, W. E.; Vazquez, C.; McLean, R. S.; Ward, M. D.; Jones, N. C.; Miller, J. S. *Chem. Commun. (Cambridge)* **1997**, 409.

(6) Buschmann, W. E.; Arif, A. M.; Miller, J. S. *Angew. Chem., Int. Ed.* **1998**, *37*, 781; *Angew. Chem.* **1998**, *110*, 813.

(7) (a) Dunbar, K. *Prog. Inorg. Chem.* **1996**, *45*, 823. (b) Meier, I. K.; Pearlstein, R. M.; Ramprasad, D.; Pez, G. *Inorg. Chem.* **1997**, *36*, 1707. (c) Carter, S. J.; Foxman, B. M.; Stuhl, L. S. *J. Am. Chem. Soc.* **1984**, *106*, 4265. (d) Towns, R. L. R.; Levenson, R. A. *J. Am. Chem. Soc.* **1972**, *94*, 4345.

10.1021/ic0012726 CCC: $20.00
Published on Web 03/09/2001

octahedral complexes, although a few are low spin.[8] From magnetic susceptibility and electron paramagnetic resonance (EPR) studies, it was unambiguously determined that $[Mn(CN)_4]^{2-}$ is indeed high-spin ($S = {}^5/_2$) with an essentially temperature-independent moment of 5.99 μ_B (5.92 μ_B predicted) and a Curie θ value of 0 K.[6]

With the discovery of $[Mn^{II}(CN)_4]^{2-}$, a synthon to develop novel magnetic 3-D networks akin to the Prussian Blue family of magnetic materials emerged. Prussian Blue, $Fe^{III}_4[Fe^{II}(CN)_6]_3 \cdot yH_2O$ ($14 < y < 16$), is the prototype of a class of 3-D network solids composed of $Fe^{II}-C-N-Fe^{III}$ linkages extended in three dimensions.[9] Several members of this class of materials magnetically order below an ordering temperature, T_c, which, in several cases, exceeds room temperature.[10]

Herein, we report on the formation of $[Mn(CN)_4]^{2-}$ in solution and the solid state, its solution behavior, and a variety of network solids formed by reacting $[Mn(CN)_4]^{2-}$ with first-row transition metal dications.

Experimental Section

All manipulations were performed under N_2 or argon using standard Schlenk techniques or a Vacuum Atmospheres inert atmosphere DriLab. Dichloromethane was dried and distilled under N_2 from CaH_2. Acetonitrile was dried and twice distilled under N_2 from CaH_2. Diethyl ether (Et_2O) and tetrahydrofuran (THF) were dried and distilled under N_2 from sodium benzophenone ketyl radical. $[M^{II}(NCMe)_6][TFPB]_2$ (M = V, Cr, Mn, Fe, Co, Ni; TFPB = $B[C_6H_3(CF_3)_2]_4$) salts,[11] $K_3[Mn^{III}(CN)_6]$,[12a] and $[PPN]_3[Mn^{III}(CN)_6]$[12b] [$PPN^+ = (Ph_3P)_2N^+$] were prepared as previously described. $[Et_4N][PF_6]$ was obtained by mixing a 50 mL aqueous solution of [Et4N]Cl (Aldrich) (3.01 g, 18.2 mmol) with a 50 mL aqueous solution of $K[PF_6]$ (Alfa) (3.34 g, 18.2 mmol). The white precipitate was filtered off, washed with water several times, air-dried, recrystallized from a minimum amount of hot MeOH, and dried in vacuo.

$[Fe(C_5H_5)_2]\{B[C_6H_3(CF_3)_2]_4\}$. A 50 mL Et_2O solution containing *p*-benzoquinone (1.29 mmol, 0.140 g) and HCl (2.6 mmol, 2.6 mL as a 1.0 M Et_2O solution) was added via cannula to an Et_2O solution (40 mL) containing $K\{B[C_6H_3(CF_3)_2]_4\}$ (2.355 mmol, 2.124 g) and $Fe(C_5H_5)_2$ (2.59 mmol, 0.482 g). The reaction mixture immediately turned blue in color. The product precipitated from solution by addition of hexanes, was isolated by vacuum filtration, and then was recrystallized from Et_2O/hexanes and dried in vacuo. Yield: 1.985 g of deep blue needles (80% yield based on $K\{B[C_6H_3(CF_3)_2]_4\}$). IR (Nujol): 3118, 1608, 1355, 1279, 1164, 1141, 1122, 1098, 950, 929, 892, 853, 838, 744, 719, 712, 683, 670 cm^{-1}. Mp: 120 °C dec. Anal. Calcd for $C_{42}H_{22}BF_{24}Fe$: C, 48.09; H, 2.11. Found: C, 48.01; H, 2.20.

$[PPN]_2[Mn^{IV}(CN)_6]$. The previous method[5] was improved by adding a 1:6 MeCN/Et_2O solution (70 mL) containing $[Fe(C_5H_5)_2]\{B[C_6H_3(CF_3)_2]_4\}$ (0.7763 mmol, 0.8143 g) to a MeCN solution (35 mL) containing $[PPN]_3[Mn^{III}(CN)_6]$ (0.7763 mmol, 1.418 g) while excluding light (solutions are stable under red light). The blue color of the $[Fe(C_5H_5)_2]^+$ disappeared immediately upon mixing. Addition of another 20 mL of Et_2O with stirring initiates crystallization from solution after ~1 min. The product was allowed to settle for 30 min, isolated by vacuum filtration, and recrystallized from MeCN/Et_2O. Small, yellow platelet crystals were isolated in 90% yield. IR ν_{CN} (Nujol, MeCN): 2132 cm^{-1}. Raman ν_{CN} (solid): 2135 cm^{-1}. Mp: 142 °C dec. Anal. Calcd for $C_{78}H_{60}N_8P_4Mn$: C, 72.73; H, 4.70; N, 8.40. Found: C, 72.49; H, 4.51; N, 8.58.

$[Et_4N]_2[Mn^{IV}(CN)_6]$. A CH_2Cl_2 solution (5 mL) containing $[Et_4N]PF_6$ (0.220 mmol, 0.0606 g) was added to a CH_2Cl_2 solution (8 mL) containing $[PPN]_2[Mn^{IV}(CN)_6]$ (0.1060 mmol, 0.1366 g) while light was excluded. Et_2O (1 mL) was added, and the reaction mixture became cloudy with a precipitate. The solid was isolated by vacuum filtration and recrystallized from CH_2Cl_2/MeCN/Et_2O. Yield: 50 mg of yellow microcrystalline solid (50% yield). IR ν_{CN} (Nujol): 2132 cm^{-1}. Mp: 123 °C dec. Anal. Calcd for $C_{23.25}Cl_{0.50}H_{40.50}MnN_8$ (includes 0.25 equiv of CH_2Cl_2): C, 54.23; H, 8.28; N, 22.47. Found: C, 54.20; H, 8.74; N, 22.71.

Photochemical Preparation of $[PPN]_2[Mn^{II}(CN)_4]$. A solution of $[PPN]_2[Mn(CN)_6]$ (1.546 g, 0.8470 mmol) in 10 mL of MeCN/CH_2Cl_2, 1:1, was exposed to ambient fluorescent light until the color had changed from yellow to red. The solution was then layered with Et_2O to crystallize out 0.314 g of burgundy-red prisms (30% yield). IR ν_{CN}: 2205 cm^{-1} (Nujol), 2202 cm^{-1} (MeCN). Raman ν_{CN} (solid): 2109 cm^{-1}. Dec: 206 °C (DSC, TGA). Anal. Calcd for $C_{76}H_{60}MnN_6P_4$: C, 73.84; H, 4.82; N, 6.80. Found: C, 73.62; H, 4.97; N, 6.75.

Thermochemical Preparation of $[PPN]_2[Mn^{II}(CN)_4]$. A 50.0 mg sample of yellow $[PPN]_2[Mn(CN)_6]$ was heated in vacuo at 140 °C for 14 h. The remaining solid was pale red and 4.0% (2.0 mg) less in mass than prior to heating. Recrystallization from MeCN/CH_2Cl_2/Et_2O gave burgundy-red crystals in 90% yield. IR ν_{CN}: 2205 cm^{-1} (Nujol), 2202 cm^{-1} (MeCN). Dec: 206 °C (DSC, TGA).

$[Et_4N]_2[Mn^{II}(CN)_4]$. A solution of $[Et_4N][PF_6]$ (0.0606 g, 0.220 mmol) in 5 mL of 10:1 CH_2Cl_2/MeCN was added to a red solution of $[PPN]_2[Mn(CN)_4]$ (0.1236 g, 0.1000 mmol) in 5 mL of CH_2Cl_2, and a fine precipitate began to form. The volume was approximately doubled with Et_2O to precipitate the product. The solid was isolated by vacuum filtration and recrystallized from MeCN/CH_2Cl_2/Et_2O. Yield: 270 mg of dark burgundy-red twinned needles (64% yield). IR ν_{CN}: 2209 cm^{-1} (Nujol), 2201 cm^{-1} (MeCN). Mp: 137 °C (DSC). Dec: 248 °C (DSC, TGA). Anal. Calcd for $C_{20}H_{40}MnN_6$: C, 57.26; H, 9.61; N, 20.03. Found: C, 57.29; H, 9.53; N, 19.99.

$[PPN]_2[C_{12}N_{12}]$. A solution of $[PPN]_2[Mn(CN)_6]$ (100 mg, 0.077 mmol) in 3 mL of CH_2Cl_2 was exposed to ambient fluorescent light until the color had changed from yellow to red. This was slowly diluted with Et_2O by vapor diffusion while sitting on an optical bench for 1 month. Small pale-yellow crystals were isolated by vacuum filtration in <5% yield. IR (Nujol): $\nu_{C\equiv N}$, 2299 (m), 2176 (m) cm^{-1}; $\nu_{C=N}$, 1559 (s) cm^{-1}. UV−vis λ_{max} (CH_3CN): 288 nm (ϵ = 24 900 M^{-1} cm^{-1}). Anal. Calcd for $C_{84}H_{60}N_{14}P_4$: C, 72.62; H, 4.35; N, 14.11. Found: C, 72.20; H, 4.50; N, 13.94.

$[PPN][C_4N_4]$. A solution of $[PPN]_4[Mn(CN)_6]$ (800 mg) in 22.5 mL of 1.25:1 CH_2Cl_2/Et_2O was allowed to stand for 10 months in ambient fluorescent light. The red solution was removed from a small amount of red precipitate and the solution reduced in volume to approximately 10 mL under reduced pressure. Fresh diethyl ether (10 mL) was layered onto the solution, and deep-red prisms grew within 4 weeks. The crystals were isolated by vacuum filtration yielding 1.1 mg of $[PPN][C_4N_4]$. IR (Nujol): $\nu_{C\equiv N}$, 2191 (m), 2160 (m) cm^{-1}; $\nu_{C=N}$, 1524 (m) cm^{-1}. Composition was determined by single-crystal X-ray structural analysis.

(8) Huheey, J. E.; Keiter, E. A.; Keiter, R. L. *Inorganic Chemistry*, 4th ed.; Harper Collins, 1993; p 403. Byrne, E. K.; Theopold, K. H. *J. Am. Chem. Soc.* **1989**, *111*, 3887. Arnold, J.; Wilkinson, G.; Hussaun, B.; Hursthouse, M. B. *J. Chem. Soc., Chem. Commun.* **1988**, 1349. Stavropoulos, P.; Savage, P. D.; Tooze, R. P.; Wilkinson, G. *J. Chem. Soc., Dalton Trans.* **1987**, 557.

(9) Ludi, A.; Güdel, H. U. *Struct. Bonding* **1973**, *14*, 1.

(10) (a) Ferlay, S.; Mallah, T.; Ouahès, R.; Veillet, P.; Verdaguer, M. *Inorg. Chem.* **1999**, *38*, 229. Holmes, S. D.; Girolami, G. *J. Am. Chem. Soc.* **1999**, *121*, 5593. Hatlevik, Ø.; Buschmann, W. E.; Zhang, J.; Manson, J. L.; Miller, J. S. *Adv. Mater.* **1999**, *11*, 914. Dujardin, E.; Ferlay, S.; Phan, X.; Desplanches, C.; Moulin, C. C. D.; Sainctavit, P.; Baudelet, F.; Dartyge, E.; Veillet, P.; Verdaguer, M. *J. Am. Chem. Soc.* **1998**, *120*, 11347. Ferlay, S.; Mallah, T.; Ouahès, R.; Veillet, P.; Verdaguer, M. *Inorg. Chem.* **1999**, *38*, 229. Verdaguer, M.; Bleuzen, A.; Train, C. Garde, R.; Debiani, F. F.; Desplanches, C. *Philos. Trans. R. Soc. London (A)* **1999**, *357*, 3159. (b) E.g.: Buschmann, W. E.; Paulson, S. C.; Wynn, C. M.; Girtu, M.; Epstein, A. J.; White, H. S.; Miller, J. S. *Adv. Mater.* **1997**, *9*, 645; *Chem. Mater.* **1998**, *10*, 1386. Ferlay, S.; Mallah, T.; Ouahes, R.; Veillet, P.; Verdaguer, M. *Nature* **1995**, *378*, 701. Entley, W. R.; Treadway, C. R.; Girolami, G. S. *Mol. Cryst. Liq. Cryst.* **1995**, *237*, 153. Mallah, T.; Thiébaut, S.; Verdaguer, M.; Veillet, P. *Science* **1993**, *262*, 1554. Greibler, W. D.; Babel, D. *Z. Naturforsch.* **1982** *87b*, 832.

(11) Buschmann, W. E.; Miller, J. S. *Chem.—Eur. J.* **1998**, *4*, 1731.

(12) (a) Brauer, G. *Handbook of Preparative Inorganic Chemistry*, 2nd ed.; Academic Press: New York, 1965; Vol. 2, p 1473. (b) Buschmann, W. E.; Liable-Sands, L.; Rheingold, A. L.; Miller, J. S. *Inorg. Chim. Acta* **1999**, *284*, 175. (c) Alexander, J. J.; Gray, H. B. *J. Am. Chem. Soc.* **1968**, *90*, 4260.

α-$Mn^{II}[Mn^{II}(CN)_4]$. Solid $[PPN]_2[Mn(CN)_4]$ (0.0925 mmol, 0.1144 g) and $[Mn(NCMe)_6][TFPB]_2$ (0.0925 mmol, 180 mg) were added together in a 25 mL flask with magnetic stirring. Et_2O (10 mL) was added with stirring, which was followed by addition of 5 mL of CH_2Cl_2. A red-brown solid was observed after stirring for 4 h, and the mixture was stirred for an additional 0.5 h. The product was isolated by vacuum filtration and washed several times with Et_2O. The solid was dried in vacuo for approximately 0.5 h, producing a fine red-brown powder in quantitative yield. IR (Nujol) ν_{CN}: 2170 cm^{-1}. This is the first product formed without thermal treatment. TGA revealed a continual weight loss from ~30 to 500 °C indicating decomposition.

On one occasion the β-$Mn^{II}[Mn^{II}(CN)_4]$ was isolated using this identical procedure, as evidenced by a different IR pattern and magnetic properties. IR (Nujol) ν_{CN}: 2159 cm^{-1}.

α-$Mn^{II}[Co^{II}(CN)_4]$. Solid samples of $[PPN]_2[Mn(CN)_4]$ (0.0467 mmol, 0.0578 g) and $[Co^{II}(NCMe)_6][SbF_6]_2$ (0.0467 mmol, 0.0363 g) were added together in a 20 mL flask with a magnetic stir bar. THF (3 mL) was added with stirring followed by the addition of 3 mL of CH_2Cl_2. A blue-green solid was observed precipitating from solution soon after and the reaction mixture stirred for 1 h. The product was isolated by vacuum filtration followed by subsequent washing with THF and CH_2Cl_2 and dried in vacuo for 2 h. IR (Nujol) ν_{CN}: 2210 (w), 2158 (sh), 2114 (s) cm^{-1}. TGA revealed a continual weight loss from ~30 to 500 °C indicating decomposition.

β-$Co[Mn(CN)_4]$ was produced by thermolysis of a bulk sample of the α-phase at 135 °C for 2 h. IR (Nujol) ν_{CN}: 2158 (s) cm^{-1}.

$Mn^{II}[Ni^{II}(CN)_4]$. Solid samples of $[PPN]_2[Mn(CN)_4]$ (0.128 mmol, 0.1582 g) and $[Ni(NCMe)_4][O_3SCF_3]_2$ (0.128 mmol, 77.2 mg) were added together in a 20 mL flask with a stir bar. Approximately 6 mL of THF was added, resulting in a pale yellow-green solution. After stirring for about 0.5 h, 2 mL of CH_2Cl_2 was quickly added and precipitation of a pale yellow solid occurred. The product was isolated by vacuum filtration, washed numerous times with CH_2Cl_2, and dried in vacuo for 1 h. IR (Nujol) ν_{CN}: 2159 cm^{-1}. TGA revealed a continual weight loss from ~30 to 500 °C indicating decomposition.

Spectroscopic Measurements. Infrared spectra were obtained on a Bio-Rad FTS-40 Fourier transform spectrometer in the range 600−4000 ± 1 cm^{-1}. Solids were analyzed as Nujol mulls sandwiched between NaCl plates and solutions measured in a NaCl cell with a 0.100 mm path length. Variable-temperature infrared studies were carried out using a custom-made heating attachment with an Ondyn temperature controller in the standard transmittance configuration. Spectra were recorded between 25 and 175 °C after allowing the temperature to equilibrate for 10 min or greater prior to acquisition.

Raman spectra were obtained using a SPEX 1877, 0.6 m triple spectrometer equipped with a SPEX Spectrum-1 CCD detector. The radiation source was a Ti-sapphire Coherent 890 tunable laser energized by a Coherent Innova 300 Ar ion laser. An excitation line of 764.925 nm was used.

UV−vis−near-IR spectra were made using a Cary-17D spectrophotometer with an On-Line Instrument Systems Inc. interface between 225 and 800 nm. Solution spectra were measured in 1 or 5 cm path length airtight quartz UV cells using freshly prepared MeCN solutions.

Electron paramagnetic resonance (EPR) spectra were obtained with a Bruker, model ESP 300E, spectrometer equipped with a X-band microwave bridge with a model ER 041 XK frequency counter, and an Oxford He cryostat controller. Measurements were made between ambient temperature and 78 K. Measurements were made on solutions in CH_2Cl_2 or CH_2Cl_2/MeCN mixtures in standard 3 mm fused quartz EPR tubes.

X-ray Diffraction. The single-crystal X-ray structure of $[PPN][C_4N_4]$ was determined on a Bruker CCD diffractometer. Table 1 and the Supporting Information summarize the data collection and refinement. X-ray powder diffraction spectra were taken on a Rigaku Miniflex diffractometer model 1GC2 (Cu Kα). The reflection 2θ values were corrected with an internal crystalline silicon standard.

Magnetic Measurements. Magnetic susceptibility measurements were made between 2 and 300 K with a Quantum Design MPMS-5XL SQUID ac/dc magnetometer equipped with the ultralow-field (~0.005 Oe) accessory, reciprocating sample measurements system, and continuous low-temperature control with enhanced thermometry features. Zero-field-cooled measurements were made in a residual field of −0.002 ± 0.001 to 0.002 ± 0.001 Oe based on the fluxgate response. Ac-susceptibility measurements were carried out at low temperature (2−40 K) using $H_{dc} = 0$ and 1 Oe oscillating fields of 10, 100, and 1000 Hz. The samples were loaded in an inert atmosphere glovebox in a Delrin airtight holder. All magnetic data were corrected for the sample holder contribution and for core diamagnetism as calculated from Pascal's constants. A value of -65×10^{-6} emu/mol was used for $[Mn(CN)_4]^{2-}$.

Thermal Analysis. Thermal properties of materials were studied on a TA Instruments model 2910 differential scanning calorimeter (DSC) and a TA Instruments model 2050 thermal gravimetric analyzer (TGA). Temperature control is maintained between −150 and 500 °C, and ambient and 1000 °C for the DSC and TGA instruments, respectively. The TGA is located in a Vacuum Atmospheres inert atmosphere glovebox in order to study oxygen and moisture sensitive samples. TGA samples were handled in an Ar atmosphere and heated under a N_2 purge. DSC samples were weighed and hermetically sealed under Ar in aluminum pans. Heating rates were 15 °C/min for TGA and 5 °C/min for DSC experiments unless otherwise noted in the text. Elemental analyses were performed at Atlantic Microlabs, Inc.

Results and Discussion

Monitoring the photolysis of $[Mn^{IV}(CN)_6]^{2-}$ in CH_2Cl_2 by IR shows the intensity of $[Mn^{IV}(CN)_6]^{2-}$, $\nu_{CN} = 2135$ cm^{-1} (Figure 1a, peak **I**), decreasing and the detectable production of $[Mn^{II}(CN)_4]^{2-}$, $\nu_{CN} = 2202$ cm^{-1} (peak **II**), occurring by exposure to ambient light at room temperature. An additional absorption grows in at 1562 cm^{-1} ($\nu_{C=N}$) accompanied by a shoulder around 2170 cm^{-1} ($\nu_{C\equiv N}$), (peaks **III** and **IV**) ascribed to the formation of {(1,1,2,2-tetracyano-1,2-ethanediyl)bis-[imino(cyanomethylene)]}bis[cyanamide] ion(2−), $[C_{12}N_{12}]^{2-}$ (**2**), reported previously.[13] The integrated areas of peaks **I**, **II**, and **III** are plotted as a function of time, *t*, in Figure 1b. The observed rate for the disappearance of $[Mn^{IV}(CN)_6]^{2-}$, **I**, is fit best to an exponential first-order rate constant during the first 125 min [$\ln(A_0/A)$ vs *t* has a linear slope of 0.0106] whereas the production of **II** fits best to a zero-order rate constant with a linear slope of 0.00107 fit to the first 165 min. The rate of photolysis is reduced as the concentration of the light-absorbing $[Mn^{II}(CN)_4]^{2-}$ increases, which reduces the number of photons transmitted through solution, adding a significant nonlinear component to the observed rate after ~125 min. The formation of $[Mn^{II}(CN)_4]^{2-}$, **II**, is not detected during the first 10 min of photolysis, and $[C_{12}N_{12}]^{2-}$, **III**, is not detected during the first 65 min.

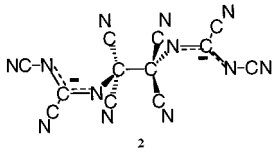

2

The photoinduced decomposition of $[Mn^{IV}(CN)_6]^{2-}$ in MeCN is more complex with respect to CH_2Cl_2 as three new cyano species are resolved in the IR, Figure 2a. The production of $[C_{12}N_{12}]^{2-}$ does not occur under these conditions. The initial 2132 cm^{-1} absorption of $[Mn^{IV}(CN)_6]^{2-}$ (peak **V**) rapidly decreases in intensity while broader absorptions at 2100 cm^{-1} (peak **VI**) and at 2141 cm^{-1} (peak **VII**) increase in intensity. The broad absorption for $[Mn^{II}(CN)_4]^{2-}$ starts to grow in at 2200 cm^{-1} (peak **VIII**) and is soon accompanied by another absorption growing in at 2086 cm^{-1} (peak **IX**). The integrated areas of peaks **V**−**IX** vs *t* are plotted in Figure 2b. The observed rate

(13) Buschmann, W. E.; Arif, A. M.; Miller, J. S. *J. Chem. Soc., Chem. Commun.* **1995**, 2343.

Table 1. Crystallographic Details for $[PPN][C_4N_4]$

chem formula	$C_{40}H_{30}N_5P_2$	formula mass, Da	642.63
a	18.6314(2) Å	space group	*I*2/*a*
b	9.1926(1) Å	*T*	293 K
c	20.8006(1) Å	λ	0.71073 Å
α	90°	ρ_{calcd}	1.248 g cm^{-3}
β	106.176(2)°	μ	0.163 mm^{-1}
γ	90°	$R_1(F_o)^a$	0.0510
V	3421.50(5) Å^3	$R_w(F_o^2)^b$ =	0.1427
Z	4		

$^a \Sigma||F_o| - |F_c||/\Sigma|F_o|$. $^b \{\Sigma[w(F_o^2 - F_c^2)^2]/\Sigma w(F_o^2)^2\}^{1/2}$.

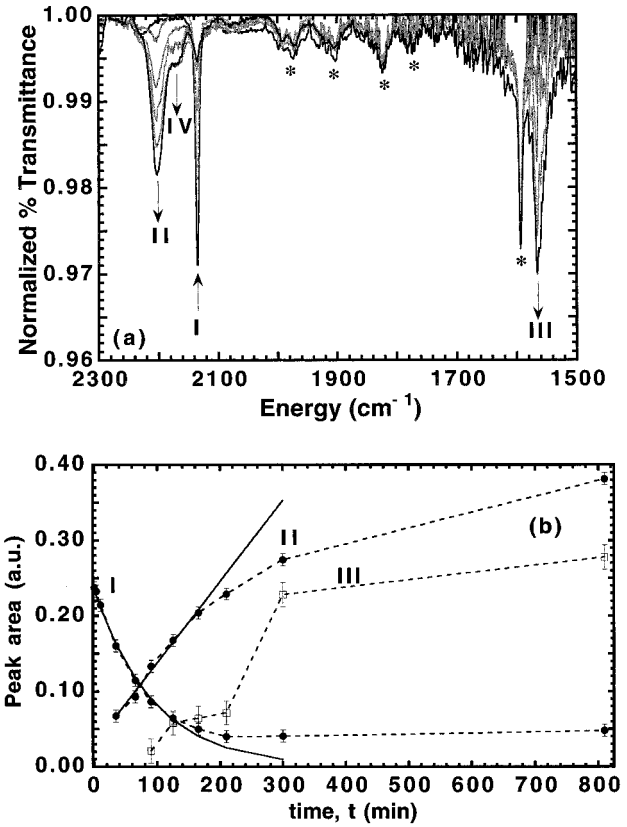

Figure 1. (a) IR spectra of a 10.0 mM CH_2Cl_2 solution of $[PPN]_2[Mn^{IV}(CN)_6]$ exposed to ambient light for 810 min. Peak **I**, $[Mn^{IV}(CN)_6]^{2-}$, loses intensity while peaks **II**, $[Mn^{II}(CN)_4]^{2-}$, **III** and **IV**, $[C_{12}N_{12}]^{2-}$, grow in. Peaks marked with an asterisk (*) are due to the aromatic rings of the $[PPN]^+$. (b) Integrated areas for peaks **I**−**III** vs *t*. Curve fits (solid lines) for peak **I** (exponential) and **II** (linear) are extrapolated beyond the fitted range.

for the disappearance of **V** fits best to an exponential first-order rate constant during the first 48 min [$\ln(A_0/A)$ vs *t* has a linear slope of 0.115], and the production of $[Mn^{II}(CN)_4]^{2-}$, **VIII**, fits best to a zero-order rate constant with a linear slope of 0.003 74 over the first 60 min after an induction period of ~6 min. In this case, the concentration of the light-absorbing $[Mn^{II}(CN)_4]^{2-}$ does not increase appreciably before $[Mn^{IV}(CN)_6]^{2-}$ is consumed by photolysis. There are, however, two species, peaks **VI** and **VII**, that are formed as soon as photolysis has begun. Peak **VII** grows to a constant intensity in ~75 min, but peak **VI** first increases, plateaus, and then decreases continuously. Peak **IX** is observed after $[Mn^{IV}(CN)_6]^{2-}$, **V**, is nearly undetected and peak **VI** reaches its maximum intensity.

The observed rate of photoinduced decomposition for $[Mn^{IV}(CN)_6]^{2-}$ is first order in both CH_2Cl_2 and MeCN with nearly an order of magnitude greater rate in MeCN. This difference in rate is likely due to MeCN being a coordinating solvent that can stabilize the intermediate manganocyanide species and also

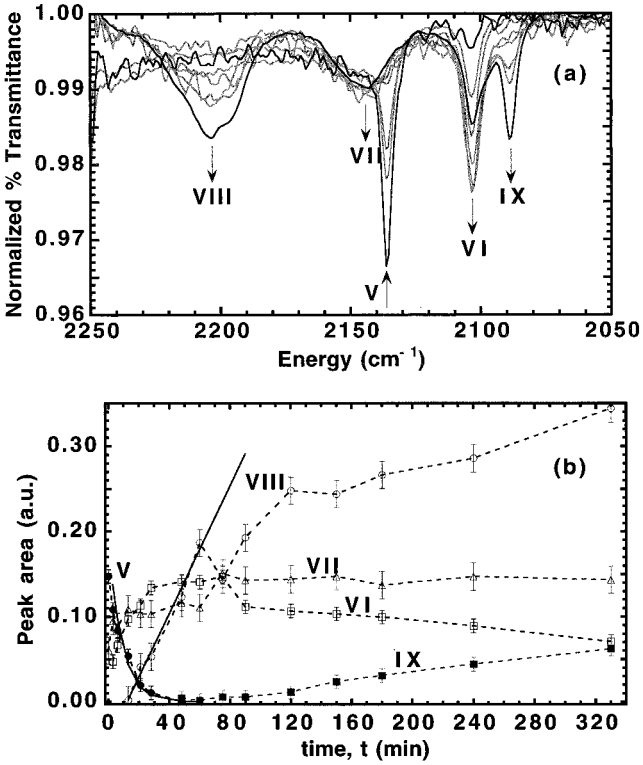

Figure 2. (a) IR spectra of a 10.0 mM MeCN solution of $[PPN]_2[Mn^{IV}(CN)_6]$ exposed to ambient light for 330 min. Peak **V**, $[Mn^{IV}(CN)_6]^{2-}$, loses intensity while peaks **II** and **III** gain intensity, then peaks **VIII**, $[Mn^{II}(CN)_4]^{2-}$, and **IX** gain intensity and **VI** loses intensity. (b) Integrated areas for peaks **V**−**IX** vs *t*. Curve fits (solid lines) for peaks **V** (exponential) and **VIII** (linear) are extrapolated beyond the fitted range.

having greater dielectric strength for solvating small fragments such as CN$^\bullet$ and CN$^-$. In MeCN formation of $[Mn^{II}(CN)_4]^{2-}$ occurs after a several minute induction period, consistent with formation of an intermediate. One intermediate is ascribed to peak **VI**, Figure 2, since this species goes through a maximum concentration partway through the photolysis before being consumed. There is evidence to suggest that this is $[Mn^{III}(CN)_6]^{3-}$, $\nu_{CN} = 2100$ cm^{-1},[12b] because it can be crystallized from these solutions in significant amounts by addition of a counter solvent. Peak **VII** appears to be a side product that is likely dimeric/oligomeric with Mn−CN−M linkages that gives rise to the 2141 cm^{-1} absorption. This absorption is within the region known for several cyano-bridging $M[Mn^{III}(CN)_6]$ compounds,[3a,14] but is too high in energy for isolated $[Mn(CN)_6]^{n-}$ ($n = 4$,[12a] 3,[12b] 2[5]). The formation of peak **IX** later in the reaction correlates with the consumption of peak **VI** and is consistent with forming NCCN, but a $[Mn^{II}(CN)_6]^{4-}$ species[2] cannot be discounted.

The photolysis in CH_2Cl_2 proceeds with formation of only the two final products, $[Mn^{II}(CN)_4]^{2-}$, **II**, and $[C_{12}N_{12}]^{2-}$, **III** and **IV**, Figure 1. The production of $[Mn^{II}(CN)_4]^{2-}$ also occurs after an induction period of several minutes suggesting that it is formed from an intermediate as well. An important comparison to make between the photolysis in CH_2Cl_2 and MeCN is that the disappearance of $[Mn^{IV}(CN)_6]^{2-}$ is first order in both cases even though the rates differ by an order of magnitude and the detectable intermediates and products are not all the same. This is evidence that loss of cyanide from the photoexcited state species, $\{[Mn^{IV}(CN)_6]^{2-}\}^*$, is the rate-limiting step and

(14) Ently, W. R.; Girolami, G. S. *Inorg. Chem.* **1994**, *33*, 5165; **1995**, *34*, 2262.

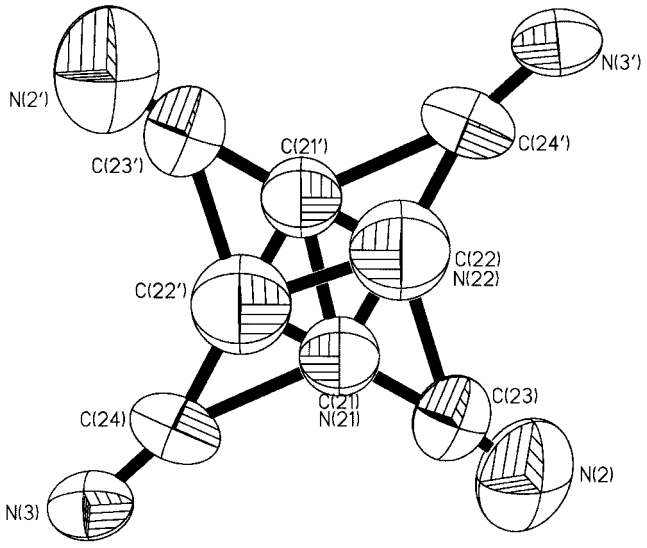

Figure 3. ORTEP and atom-labeling diagram of $[C_4N_4]^-$, **3**.

that the first-formed intermediate is not detected in either solvent. It is proposed that initial loss of a $CN^•$ leads to a very reactive $[Mn^{III}(CN)_5(solvent)]^{2-}$ intermediate that quickly undergoes reductive elimination of a second $CN^•$, dimerization, or recombination with $CN^•$ or CN^-. Coordinating solvents such as MeCN better stabilize such an intermediate and should increase the rate of $[Mn^{IV}(CN)_6]^{2-}$ photolysis. The rate of $[Mn^{II}(CN)_4]^{2-}$ production differs only by a factor of 3.5 between solvents, further supporting the rate-limiting production of an undetected intermediate species. This photolysis mechanism appears to proceed through a stepwise elimination of $CN^•$ and requires more detailed studies to elucidate it fully.

Only in CH_2Cl_2 is the production of $[C_{12}N_{12}]^{2-}$ observed in the time of photolysis, and it is presumably formed by recombination and oligomerization of $CN^•$ and CN^-.[15] In addition to formation and isolation of $[C_{12}N_{12}]^{2-}$ (**2**), a small amount of a second polycyanide oligomer, $[C_4N_4]^-$ (**3**), has been identified, and its infrared spectra and structure have been determined.

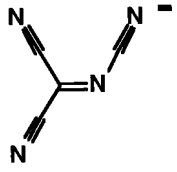

3

The structure of $[PPN][C_4N_4]$ was determined from a single-crystal X-ray diffraction study. The $[PPN]^+$ cation shows bond lengths (P−N = 1.583 Å) and angles (P−N−P = 136.2°) typical of this cation.[5,6,7c,12b] $[C_4N_4]^-$, **3**, is planar within experimental error and is positionally disordered over four equivalent sites, Figure 3. At first glance, the molecule appears to be isomorphous to TCNE (tetracyanoethylene) or $[TCNE]^{•-}$, but has different ν_{CN} absorptions as well as a deep red color. We also considered that the proposed $[C_4N_4]^-$ molecule could simply be two orientationally disordered $[C(CN)_3]^-$ anions; however, formation of a "naked" carbon atom is unlikely to occur under these circumstances. Hence, reaction of $CN^•$ radicals in solution could readily lead to $[C_4N_4]^-$, in addition to $[C_{12}N_{12}]^{2-}$. The CC and

(15) Ferris, J. P.; Donner, D. B.; Lotz, W. *J. Am. Chem. Soc.* **1972**, *94*, 6968.

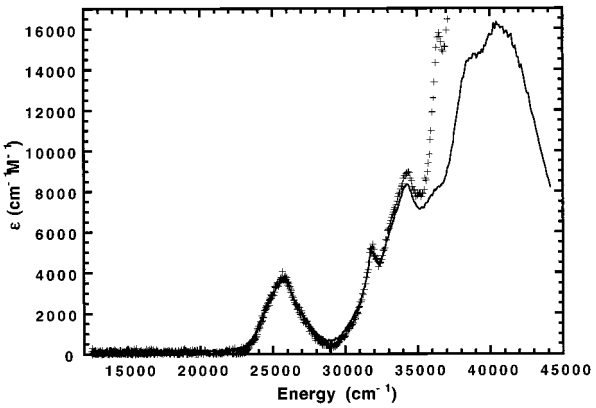

Figure 4. Electronic spectra of $[Mn^{IV}(CN)_6]^{2-}$ in MeCN (b = 5 cm) with (−) $[NEt_4]^+$ and (+) $[PPN]^+$ cations.

CN bond lengths (Å) are as follows: C(22)−N(22) 1.48(3), C(22)−C(23) 1.60(2), C(24)−N(22) 1.263(14), and C(24)−N(3) 1.032(6) Å. The large standard deviations are a result of the positional disorder, however, the observed bond distances are consistent with the $[(C{\equiv}N)_2{-}C{=}N{-}(C{\equiv}N)]^-$ formulation. Distortion of sp^2-hybridized carbons and nitrogens from the ideal angle of 120° is readily apparent from selected bond angles such as N(3)−C(24)−N(21), N(2)−C(23)−N(22), and C(24)$^{\#}$2−C(22)−C(23) which are 161.7(7)°, 145.9(13)°, and 134.6(11)°, respectively. Attempts to obtain additional material for determination of the UV−vis spectra, as well as magnetic studies, were unsuccessful.

Photochemical decomposition of $[Mn^{IV}(CN)_6]^{2-}$ in MeCN or CH_2Cl_2 is induced by an absorption into a LMCT band in the visible part of the spectrum (λ_{max} = 25 700 cm^{-1}, ϵ = 3700 cm^{-1} M^{-1}).[5] The same qualitative behavior is observed when either the $[PPN]^+$ or tetraethylammonium, $[NEt_4]^+$, cations are used, showing that the cation is not directly involved in the decomposition process. The electronic spectrum of $[NEt_4]_2[Mn^{IV}(CN)_6]$ is reported here in Figure 4 to show the higher energy CT bands that are obscured by $[PPN]^+$. Above the bands at 31 850 cm^{-1} (ϵ = 5000 cm^{-1} M^{-1}) and 34 300 cm^{-1} (ϵ = 8300 cm^{-1} M^{-1}) are three more overlapping bands positioned near 36 000 cm^{-1} ($\epsilon \sim$ 8000 cm^{-1} M^{-1}), 38 900 cm^{-1} ($\epsilon \sim$ 14 700 cm^{-1} M^{-1}), and 40 500 cm^{-1} (ϵ = 16 200 cm^{-1} M^{-1}). The overall spectrum looks like that of $[Mn^{III}(CN)_6]^{3-}$,[12b,c] but shifted to lower energy. The three lowest energy CT transitions (25 700, 31 850, 34 300 cm^{-1}) are shifted by 5300, 5250, and 6700 cm^{-1}, respectively, to lower energy going from Mn^{III} to Mn^{IV}, and the higher energy transitions are resolved. Full analysis of this data is outside the scope of this work. The important connection to point out here is that the combination of a LMCT transition being shifted into the visible and the reduction potential of the complex being favorable ($Mn^{III/IV}$ $E_{1/2}$ = 0.14 V in MeCN)[5] allows for the photoinduced reductive elimination of cyanide from $[Mn^{IV}(CN)_6]^{2-}$.

Thermal decomposition of $[Mn^{IV}(CN)_6]^{2-}$ in the solid state shows a simple transformation, with the loss of cyanogen, to produce $[Mn^{II}(CN)_4]^{2-}$. Monitoring the solid state IR spectrum of $[PPN]_2[Mn^{IV}(CN)_6]$ in Nujol at 140 °C shows the disappearance of the ν_{CN} absorption at 2132 cm^{-1} and the growing in of a broad absorption around 2185 cm^{-1}. After a bulk sample is heated to 140 °C in vacuo, the IR spectrum of the crude product shows a strong, split absorption at 2202 and 2192 cm^{-1} (Nujol). The IR spectrum of the crude product dissolved in MeCN exhibits the ν_{CN} absorption at 2202 cm^{-1} and after recrystallization at 2205 cm^{-1} (Nujol), consistent with the photochemical

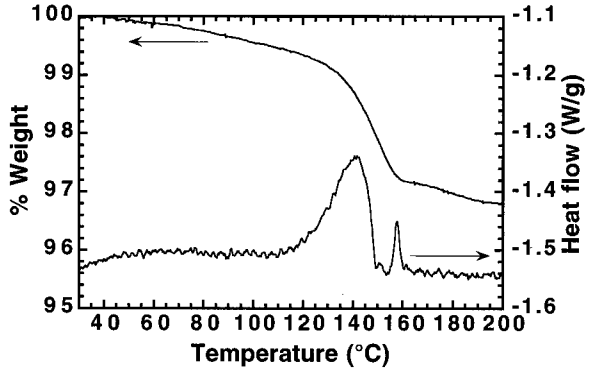

Figure 5. TGA (upper) and DSC (lower) curves for $[PPN]_2[Mn^{IV}(CN)_6]$ with heating rates of 5 and 2 °C/min, respectively.

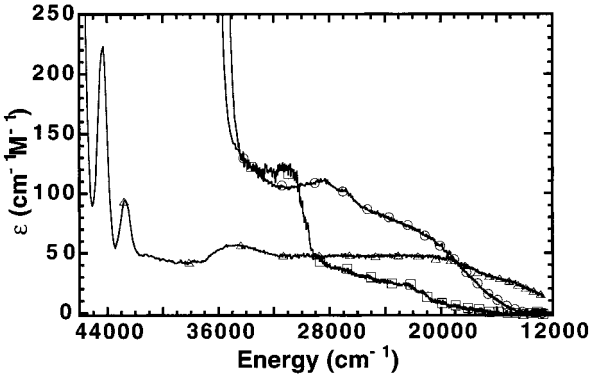

Figure 6. Electronic spectra of $[Mn^{II}(CN)_4]^{2-}$ in MeCN (b = 5 cm) with (○) $[PPN]^+$, 1.00 mM; (□) $[PPN]^+$, 0.097 mM; and (△) $[NEt_4]^+$, 1.00 mM.

preparation of $[PPN]_2[Mn^{II}(CN)_4]$. Monitoring this process by TGA consistently shows a 3.4% weight loss at T_{onset} = 136 °C, about 85% of the expected 4.04% weight loss for two CN's per Mn center, Figure 5. The DSC response shows two irreversible exotherms at T_{onset} = 122 °C (104.2 kJ/mol) and T_{onset} = 156 °C (8.2 kJ/mol). Above 250 °C there is significant decomposition and weight loss. The IR spectrum of the red thermolysis product produced in the TGA, by heating to 225 °C, exhibits single absorption bands of comparable intensity at 2198 and 1730 cm^{-1} (Nujol). The 1730 cm^{-1} absorption appears to be due to a thermolysis byproduct that can be eliminated by prolonged heating or recrystallization and accounts for the 15% excess residual mass in the TGA experiment. A curious feature of the single-crystal X-ray structure of the $[Mn^{IV}(CN)_6]^{2-}$ is that one of the three crystallographically unique cyanide ligands, C(3)N(3), has thermal parameters that are significantly greater than those of the other two cyanides.[5] It may be reasonable to expect that this C(3)N(3) is involved with the thermal Mn−CN bond homolysis.

$[PPN]_2[Mn^{II}(CN)_4]$ is most easily prepared from the reductive decomposition of $[PPN]_2[Mn^{IV}(CN)_6]$ by thermolysis in vacuo and subsequent recrystallization. It is fairly oxygen stable in the solid state and in dry aprotic solvents, but readily hydrolyzes in protic media as evidenced by a change in color from deep red to pale green. The anion also demonstrates redox stability over a wide range of potentials (ca. ±2 V) in MeCN. Details of the tetrahedral $[PPN]_2[Mn^{II}(CN)_4]$ structure, high-spin state, and room temperature solution EPR have been published previously.[6] The issue of cyanide ligand lability will be discussed here due to its significance during the formation of lattice structures with divalent first-row transition metals.

In contrast to $[Mn^{IV}(CN)_6]^{2-}$, Figure 4, and $[Mn^{III}(CN)_6]^{3-}$,[12b] the electronic spectrum of $[Mn^{II}(CN)_4]^{2-}$ changes with cation substitution and concentration, Figure 6. Significant differences appear at energies lower than 33 000 cm^{-1} and prevent assignments of d−d ligand-field transitions. The concentration-dependent absorptions are intense relative to the normal ligand-field transition intensities expected (ϵ < 10 cm^{-1} M^{-1}), suggesting the presence of aggregation or a change in geometry in solution. The difference in electronic spectra between cations may be due to differences in the cations' ability to solubilize different types/sizes of aggregates. In any case the electronic spectrum observed for $[Mn^{II}(CN)_4]^{2-}$ is atypical for isolated tetrahedral or octahedral Mn^{II} ions.[16] Solvent and cation effects have been reported for Co^{II} cyanide solutions in MeCN; however, unlike $[Mn^{II}(CN)_4]^{2-}$ the solution species of Co are detectable by IR and are thought to be monomeric.[17]

The solution EPR spectrum of $[PPN]_2[Mn^{II}(CN)_4]$ in CH_2Cl_2 changes with concentration at room temperature as previously described.[6] Below 1 mM concentration the EPR spectrum exhibits the expected isotropic six-line hyperfine interaction for ^{55}Mn ($I = {}^5/_2$) centered at g = 2.003 ($\langle|A|\rangle$ = 71 G). Above 1 mM concentration the Mn hyperfine signal broadens significantly and a very narrow 11-line resonance ($|A|$ = 1.6 G) of much weaker intensity grows in and is centered at the same g value. When a solution of $[A]_2[Mn^{II}(CN)_4]$ (A = PPN, NEt_4N) (≤1 mM) is quenched to 78 K, the spectrum changes shape and the g value increases to 2.012 ($\langle|A|\rangle$ = 71 G), Figure 7a. The concentration and temperature-dependent responses of the electronic and EPR spectra are reversible.

The strongest evidence for aggregation is in the EPR spectra. The frozen solution EPR spectrum for $[PPN]_2[Mn^{II}(CN)_4]$, Figure 7a, is nearly the same as for $[PPN]_2[Mn^{IV}(CN)_6]$ (g = 1.996, $\langle|A|\rangle$ = 68 G), Figure 7b, except the g value is greater. $[PPN]_2[Mn^{IV}(CN)_6]$ has no dramatic temperature dependence on its EPR line shape.[5] The similarity in line shapes and difference in g values between the $[Mn^{II}(CN)_6]^{2-}$ and $[Mn^{IV}(CN)_4]^{2-}$ frozen EPR spectra strongly suggest that $[Mn^{II}(CN)_4]^{2-}$ can become octahedral by some mechanism of aggregation. This could be either axial nitrile coordination of two $[Mn^{II}(CN)_4]^{2-}$ ions, i.e., **4**, or forming a $[Mn^{II}(CN)_6]^{4-}$ (low-spin, $S = {}^1/_2$) species by scavenging CN^- via linkage isomerization[3a,18] of bridging cyanides in **4** or free CN^- in solution. For a low-spin octahedral or square planar d^5 configuration contributions of spin−orbit coupling are greater than for an octahedral d^3 configuration and will result in an increase in g-value.[19a,b] Isolated square planar $[Mn^{II}(CN)_4]^{2-}$ is ruled out because it should exhibit an anisotropic spectrum with axial and equatorial **g** tensors. Nonetheless, the reaction of $[PPN]_2[Mn^{II}(CN)_4]$ with pyridine or [PPN]CN in CH_2Cl_2 yields only the tetrahedral Mn^{II} upon recrystallization. This observation supports the notion that a hexacoordinate species is relatively short-lived in solution.

(16) Figgis, B. N. *Introduction to Ligand Fields*; John Wiley-Interscience: New York, 1966; Chapter 9.

(17) Carter, S. J.; Foxman, B. M.; Stuhl, L. S. *Inorg. Chem.* **1986**, *25*, 2888.

(18) Reguera, E.; Bertrán, J. F.; Nuñez, L. *Polyhedron* **1994**, *10*, 1619. Brown, D. B.; Shriver, D. F. *Inorg. Chem.* **1969**, *8*, 37. Shriver, D. F.; Shriver, S. A.; Anderson, S. E. *Inorg. Chem.* **1965**, *4*, 725. (b) Brown, D. B.; Shriver, D. F.; Schwartz, L. H. *Inorg. Chem.* **1968**, *7*, 77. Buschmann, W. E.; Ensling, J.; Gütlich, P.; Miller, J. S. *Chem.—Eur. J.* **1999**, *5*, 3019.

(19) (a) Drago, R. S. Physical Methods for Chemists, 2nd ed.; Saunders College Pub.: Ft. Worth, TX, 1992; Chapter 10. (b) Figgis, B. N. In *Comprehensive Coordination Chemistry*; Wilkinson, G., Ed.; Pergamon: New York, 1987; Vol. 1, Chapter 6.

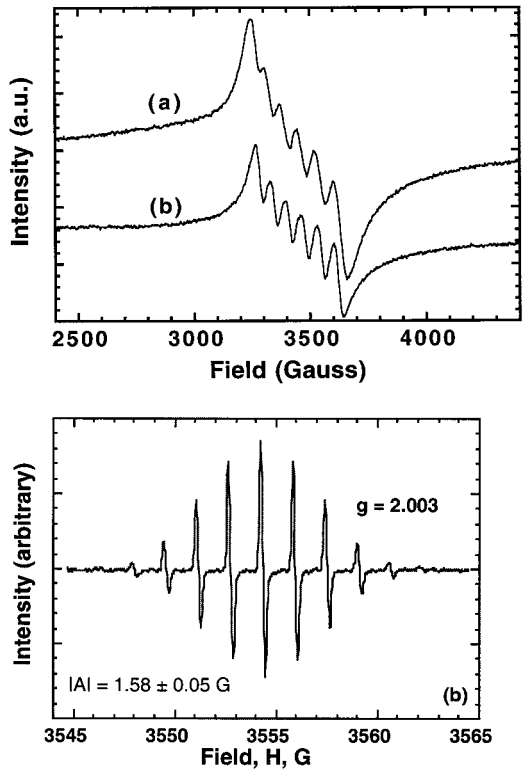

Figure 7. Frozen solution (1.00 mM, CH_2Cl_2) EPR spectra of $[PPN]_2[Mn^{II}(CN)_4]$ (a), $g = 2.012$, $|A| = 71$ G, and $[PPN]_2[Mn^{IV}(CN)_6]$ (b), $g = 1.996$, $|A| = 68$ G. Spectra (offset) were measured under the same conditions at 78 K and 9.646 GHz with the relative intensities preserved.

As noted above, a unique EPR active species becomes apparent above 1 mM concentration at room temperature while the isotropic Mn^{II} hyperfine signal broadens and becomes unobservable above ~1.5 mM.[6] These observations are consistent with spin relaxation on Mn becoming faster than the time scale of the experiment due to either intermolecular spin−spin or dipolar relaxation processes. The dramatic dependence of the EPR response on both temperature and concentration is consistent with a hexacoordinate Mn^{II} equilibrium species due to intermolecular significant interactions.

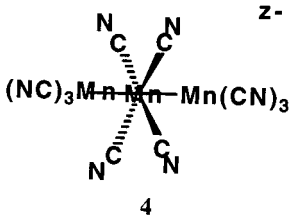

4

3-D $M^{II}[Mn^{II}(CN)_4]$ Lattice Compounds. The inherent lability of the $[Mn^{II}(CN)_4]^{2-}$ ion in solution is a challenging issue in the preparation of single-component $M[Mn(CN)_4]$ (M = Cr, Mn, Fe, Co, Ni) sphalerite (diamond-like) lattices, akin to $Zn^{II}(CN)_2$,[20] as potential magnetic materials. In numerous cases more than one cyano-containing product is formed when equimolar amounts of $[PPN]_2[Mn^{II}(CN)_4]$ and $[M^{II}(NCMe)_6]^{2+}$ salts are combined as indicated by IR spectroscopy and significant variations in magnetic behavior from sample to sample. Many attempts were made by varying the solvent conditions, concentrations, and reaction temperatures to isolate pure, single-phase materials. The three best-characterized systems (M = Mn, Co, Ni) are presented.

Mn. The homometallic α-$Mn^{II}[Mn^{II}(CN)_4]$ is the first example of a paramagnetic sphalerite lattice. Details of the structure and magnetic behavior have previously been published.[21] The reaction of $[PPN]_2[Mn^{II}(CN)_4]$ and $[Mn^{II}(NCMe)_6][TFPB]_2$ in MeCN forms α-$Mn^{II}[Mn^{II}(CN)_4]$ as a red-brown precipitate. The IR spectrum of the initial sample suggests a pure structurally ordered material of high symmetry, i.e., a single, sharp ν_{CN} band is observed at 2170 cm^{-1}. This is reduced by 32 cm^{-1} relative to $[Mn^{II}(CN)_4]^{2-}$, suggesting weakening of the C≡N bond upon coordination of its nitrogen atom to high-spin Mn^{II}. This is the opposite effect observed for $Zn^{II}(CN)_2$ (2217 cm^{-1}), which significantly increases in frequency relative to that found for $K_2[Zn^{II}(CN)_4]$ (2149 cm^{-1}).[22] Thermogravimetric analysis of initially formed α-$Mn^{II}[Mn^{II}(CN)_4]$ between 25 and 500 °C shows a continuous weight loss of about 27% between ~40 and 500 °C. Mass spectrometry has confirmed the loss of CN^-, HCN, and $(CN)_2$ with no evidence for the presence or loss of solvents.

The unit cell parameter of $a = 6.123$ Å has been determined for α-$Mn^{II}[Mn^{II}(CN)_4]$ using the $P\bar{4}3m$ space group of $Zn^{II}(CN)_2$ ($a = 5.901$ Å) as a structural model.[21,23a] This assumes an ordered arrangement of cyano ligands, i.e., MnC_4 and MnN_4 coordination spheres. Alternatively, a random orientation of cyano ligands, i.e., MnC_nN_{4-n} ($n = 1, 2, 3, 4$) coordination sphere, may occur resulting in the lower-symmetry space group $Pn\bar{3}m$, which has been proposed for ZnC_nN_{4-n}[23a] and observed for the CdC_nN_{4-n}[23b] by ^{113}Cd NMR. The unit cell, primitive space group, and experimentally determined density[21] are consistent with an interpenetrating 3-D sphalerite-type network structure for α-$Mn^{II}[Mn^{II}(CN)_4]$. The lack of solvent molecules in the lattice after preparation is consistent with this lattice type having no large cavities. By comparison, a noninterpenetrating lattice yields a face-centered cubic structure (space group $F\bar{4}3m$) and a larger unit cell, such as 11.609 Å, reported for $[NMe_4][Cu^{I}Zn^{II}(CN)_4]$ in which the $[NMe_4]^+$ cation occupies the open lattice cavities.[20]

α-$Mn^{II}[Mn^{II}(CN)_4]$ exhibits strong antiferromagnetic coupling ($\theta = -240$ K) and order as an antiferromagnet below its Néel temperature, $T_N \approx 65$ K.[21] A complication in evaluating this material is the presence of what is estimated to be about 9.5% paramagnetic, or weakly coupled, high-spin Mn^{II} impurity. As discussed above, there is significant oligomerization of $[Mn^{II}(CN)_4]^{2-}$ in solution and such multinuclear species are subject to being coprecipitated with the bulk of the lattice compound. Dimers or trimers of Mn centers would correspond to 4.7% and 3.2%, respectively, of chemical impurity in the material. The estimated level of Mn^{II} impurity seems to be reasonable in light of the significant changes in electronic and EPR responses for $[Mn^{II}(CN)_4]^{2-}$ with concentration, vide infra.

A second, β-$Mn[Mn(CN)_4]$ phase was isolated from CH_2Cl_2, albeit on one occasion, and has a ν_{CN} absorption at 2159 cm^{-1} along with a trace amount of coordinated MeCN showing weak bands at 2308 and 2279 cm^{-1}. The magnetic susceptibility of the β-phase, Figure 8, is similar to the α-phase, showing that there is not a significant change in the spin states of, or

(20) Hoskins, B. F.; Robson, R. *J. Am. Chem. Soc.* **1990**, *112*, 1546.
(21) Manson, J. L.; Buschmann, W. E.; Miller, J. S. *Angew. Chem., Int. Ed.* **1998**, *37*, 783; *Angew. Chem.***1998**, *110*, 815.
(22) Nakamoto, K. *Infrared and Raman Spectra of Inorganic and Coordination Complexes*, 4th ed.; Wiley: New York, 1986; pp 274−279.
(23) (a) Kitazawa, T.; Nishikiori, R.; Kuroda, R.; Iwamoto, T. *J. Chem. Soc., Dalton Trans.* **1994**, 1029. (b) Nishikiori, S. I.; Ratcliffe, C. I.; Ripmeester, J. A. *Can J. Chem.* **1990**, *68*, 2270. Nishikiori, S. I.; Ratcliffe, C. I.; Ripmeester, J. A. *J. Chem. Soc., Chem. Commun.* **1991**, 735.

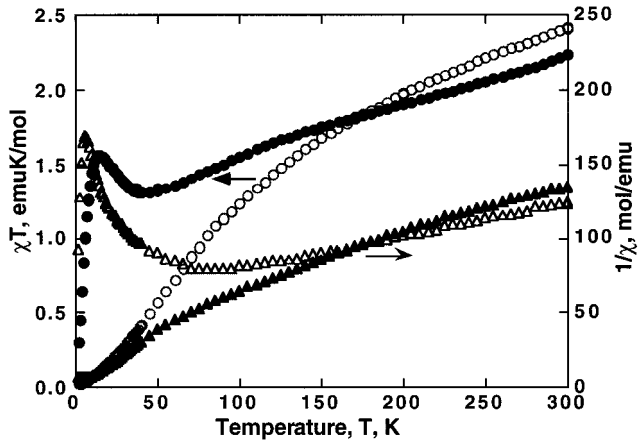

Figure 8. Temperature-dependent magnetic susceptibility of α-Mn[Mn(CN)$_4$], (○) χT, (△) $1/\chi$, and β-Mn[Mn(CN)$_4$], (●) χT, (▲) $1/\chi$.

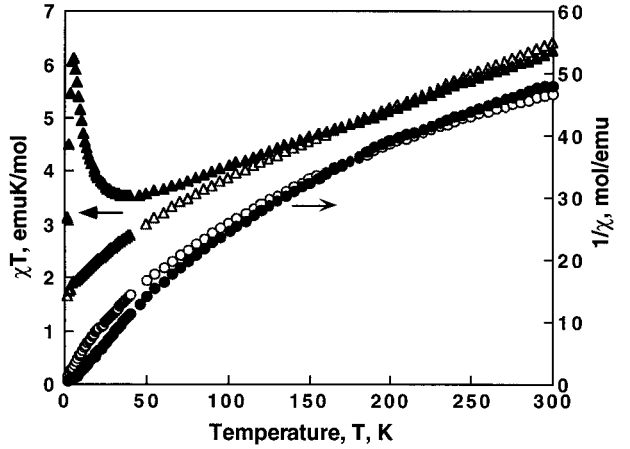

Figure 9. Temperature-dependent magnetic susceptibility of α-Mn^{II}[Co^{II}(CN)$_4$], (○) $1/\chi$, (△) χT, and β-Mn^{II}[Co^{II}(CN)$_4$], (●) $1/\chi$, (▲) χT.

short-range coupling between, Mn centers. There is no evidence, however, of long-range order above 2 K. The IR data suggests that there is open space or coordination sites in the material (by the presence of solvent) that are not available in the interpenetrating sphalerite-type structure of α-Mn^{II}[Mn^{II}(CN)$_4$]. These observations and the results for β-Mn^{II}[Co^{II}(CN)$_4$] (ν_{CN} = 2158 cm^{-1}) described below are good indications that β-Mn^{II}[Mn^{II}(CN)$_4$] is a noninterpenetrating network solid with tetrahedral [Mn^{II}(CN)$_4$]$^{2-}$ ions. Moreover the [Mn(CN)$_4$]$^{2-}$ anion is surprisingly robust in that good Lewis bases such as MeCN or pyridine do not coordinate.

Co. Linkage isomerization of cyano ligands is not expected to be an issue for spin states or geometries in α-Mn^{II}[Mn^{II}(CN)$_4$] since both Mn^{II} sites are tetrahedral and high-spin, although the local coordination sphere may contain MnN_4, MnN_3C, MnN_2C_2, and $MnNC_3$. The situation is different when exploring heterometallic materials. The reaction of [PPN]$_2$[Mn^{II}(CN)$_4$] and [Co^{II}(NCMe)$_6$][SbF$_6$]$_2$ in MeCN immediately forms a blue-green precipitate. At room temperature, this material displays its primary ν_{CN} absorption band at 2114 cm^{-1} with a shoulder around 2158 cm^{-1} and an additional weak absorption at 2210 cm^{-1}. Temperature-dependent magnetic susceptibility data, Figure 9, is evaluated for a 1:1:4 ratio of Co/Mn/CN. The observed room temperature χT value of 4.94 emu K/mol, much less than the calculated value (g = 2.00) of 6.25 emu K/mol for uncoupled high-spin Mn^{II} ($S = {}^5/_2$) and Co^{II} ($S = {}^3/_2$) tetrahedral centers, is slightly higher than the calculated 4.35 emu K/mol for Mn^{II} ($S = {}^5/_2$) and square planar Co^{II} ($S = {}^1/_2$) ions. Observed $\chi T(T)$ values are often increased for square planar Co complexes due to low-lying excited d orbitals that result in higher effective g values.[19b] A θ value of −137 K, extrapolated from $1/\chi(T)$, is indicative of strong antiferromagnetic coupling between nearest neighboring M^{II} centers through the bridging cyanides. The X-ray powder diffraction data of this material exhibits very broad features, indicative of significant structural disorder and small particle size, with a low angle peak maximum around 21.6° 2θ. This corresponds to an average M···M separation of 4.11 Å that is 1.19 and 0.96 Å shorter than the Mn···Mn separation in Mn^{II}[Mn^{II}(CN)$_4$][21] and K$_2$Mn^{II}[Mn^{II}(CN)$_6$],[14] respectively. It is even shorter than the range found for other disordered, nonaqueous M[Mn(CN)$_6$] examples.[3a,25]

The first-formed material has a color characteristic of tetrahedral Co^{II} complexes,[19b,25a] or square planar [Co^{II}(CN)$_4$]$^{2-}$,[7c] and the IR spectra suggest a mixture of CN bridging motifs. The 2114 cm^{-1} ν_{CN} absorption is consistent with either partial or full linkage isomerization (or cyanide abstraction by Co) to give the Co^{II}−CN−Mn^{II} bridging motif while the weak 2210 cm^{-1} absorption is consistent with the tetrahedral Mn^{II}−CN−Co^{II} isomer. The shoulder at 2158 cm^{-1} is also consistent with the Co^{II}−CN−Mn^{II} linkage isomer, but likely due to a different geometry. The magnetic susceptibility data supports the formulation of Mn^{II}[Co^{II}(CN)$_4$] (square planar Co^{II}) as the primary structural component. The presence of tetrahedral Co^{II} and the low-lying excited states of square planar Co^{II} are likely to be contributions to the observed room temperature χT value being 13.5% greater than the calculated. The short M···M separation given by X-ray diffraction would require unreasonably short M−C or M−N bond distances for bridging cyanide, but may reflect an interlayer separation of quasi-2-D domains structurally induced by the presence of square planar [Co^{II}(CN)$_4$]$^{2-}$. An example of this type of layered structure has been reported for Fe[Ni(CN)$_4$], which has an Fe−NC−Ni distance of 5.20 Å.[26] The above evidence leads to the assignment of the first-formed material as α-Mn^{II}[Co^{II}(CN)$_4$] with a noninterpenetrating disordered lattice network.

Upon heating, α-Mn^{II}[Co^{II}(CN)$_4$] completely transforms, irreversibly, to a second phase assigned as β-Mn^{II}[Co^{II}(CN)$_4$]. This transformation is monitored by heating an IR sample to 135 °C causing the ν_{CN} absorptions at 2210 and 2114 cm^{-1} to disappear while the only remaining absorption at 2158 cm^{-1} becomes more intense. This β-phase is considerably darker in color, and its observed room temperature χT value is 6.40 emu K/mol, Figure 9, nearly matching the above calculated value of 6.25 emu K/mol for both high-spin M^{II} tetrahedral centers. The $\chi T(T)$ for β-Mn^{II}[Co^{II}(CN)$_4$] is significantly different than for the α-phase in that it continuously decreases down to 2 K, Figure 9.

Significant differences between α- and β-Mn^{II}[Co^{II}(CN)$_4$] exist in the IR and susceptibility data and are thought to arise from the two geometric isomers possible for [Co^{II}(CN)$_4$]$^{2-}$, i.e., square planar Co^{II} for the α-phase and tetrahedral for the β-phase. Formation of the α-phase occurs first by either a linkage isomerization or CN$^-$ scavenging mechanism in the presence of the labile [Mn^{II}(CN)$_4$]$^{2-}$ ion. Monomeric square planar [Co^{II}(CN)$_4$]$^{2-}$ has been previously characterized, and its [PPN]$^+$ salt exhibits two ν_{CN} absorptions in the solid state at 2102 and 2095 cm^{-1},[7c] whereas a 1:4, Co^{II}/CN$^-$ mixture in MeCN is reported to be in a dynamic equilibrium with several

(24) Buschmann, W. E.; Miller, J. S. *Inorg. Chem.* **2000**, *39*, 2411.
(25) Cotton, F. A.; Wilkinson, G. *Advanced Inorganic Chemistry*; Wiley: New York, 1988; pp 724−732. (b) Cotton, F. A.; Wilkinson, G. *Advanced Inorganic Chemistry*; Wiley: New York, 1988; p 743.
(26) Kitazawa, T.; Funkunaga, M.; Takahashi, M.; Takeda, M. *Mol. Cryst. Liq. Cryst.* **1994**, *244*, 331.

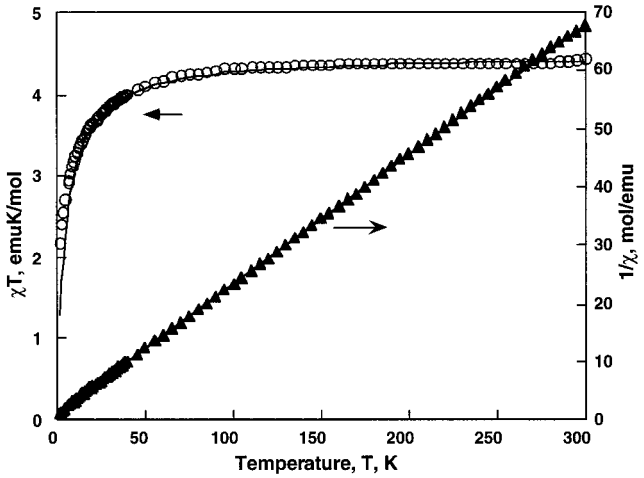

Figure 10. Temperature-dependent magnetic susceptibility of $Mn^{II}[Ni^{II}(CN)_4]$, (○) $1/\chi$, (▲) χT.

"$Co^{II}(CN)_n^{n-2}$" ($n = 2-5$) species.[17] A mixture of Mn^{II} with excess CN^- in MeCN solution does not lead to the direct formation of $[Mn^{II}(CN)_4]^{2-}$ and shows that the formation of $[Co^{II}(CN)_4]^{2-}$ is more favorable. Therefore the chemical dynamics in solution should lead to the formation of square planar $[Co^{II}(CN)_4]^{2-}$ first. Upon heating, however, the observed changes show that the geometric isomerization from square planar to tetrahedral Co^{II}, in this case, is energetically accessible and irreversible in the solid state.

Ni. Another example that demonstrates the lability of cyanide in $[Mn^{II}(CN)_4]^{2-}$ is its reaction with Ni^{II} salts. Reaction of $[PPN]_2[Mn^{II}(CN)_4]$ with either $[Ni^{II}(NCMe)_6][TFPB]_2$ or $[Ni^{II}(NCMe)_4][CF_3SO_3]_2$ in THF forms a pale yellow precipitate, upon addition of CH_2Cl_2, that exhibits a single, strong ν_{CN} band at 2159 cm^{-1}. The color of this material does not reflect the presence of tetrahedral $[Mn^{II}(CN)_4]^{2-}$, as in α-$Mn^{II}[Mn^{II}(CN)_4]$, but is consistent with yellow, square planar $[Ni^{II}(CN)_4]^{2-}$. Temperature-dependent magnetic susceptibility data for this material, Figure 10, is evaluated for a 1:1:4 ratio of Ni/Mn/CN. The observed room temperature χT value of 4.40 emu K/mol is in good agreement with a calculated value of 4.35 emu K/mol for uncoupled Mn^{II} ($S = {}^5/_2$) ions in $Mn^{II}[Ni^{II}(CN)_4]$ (square planar Ni^{II}, $S = 0$). A much greater χT value of 5.38 emu K/mol is expected for the presence of high-spin, tetrahedral Ni^{II} ($S = 1$) expected for $Ni^{II}[Mn^{II}(CN)_4]$. $1/\chi$, fit to the Curie−Weiss expression, gives a θ value of −5 K with $g = 2.02$, indicative of weak antiferromagnetic coupling between Mn^{II} centers through the bridging $[Ni^{II}(CN)_4]^{2-}$ ion. This is consistent with a significant decrease in $\chi T(T)$ below 90 K as antiferromagnetic coupling interactions increase. The X-ray powder diffraction data of this material exhibits very broad features, indicative of significant structural disorder and small particle size, with a low angle peak maximum around 18.3° 2θ. This corresponds to an average M···M separation of 4.85 Å that is 0.45 and 0.22 Å shorter than the Mn···Mn separation in $Mn^{II}[Mn^{II}(CN)_4]$[21] and $K_2Mn^{II}[Mn^{II}(CN)_6]$,[14] respectively. It is, however in the range of the average M···M separation found in other disordered, nonaqueous $M[Mn(CN)_6]$ examples.[3a,24] This short distance could reflect either a distorted Ni−CN−Mn linkage or an interlayer separation of quasi-2-D domains analogous to the reported $Fe[Ni(CN)_4]$ layered structure.[26]

The above observations lead to the conclusion that square planar $[Ni^{II}(CN)_4]^{2-}$ forms upon reaction with $[Mn^{II}(CN)_4]^{2-}$ by either abstraction or linkage isomerization[3a,18] of cyanide. The resulting material's color, ν_{CN} absorption, and room temperature χT value are consistent with the formulation of $Mn^{II}[Ni^{II}(CN)_4]$. Production of this material is likely driven by the formation of very thermodynamically stable, square planar $[Ni^{II}(CN)_4]^{2-}$.[2a,25b]

Reactions of $[PPN]_2[Mn(CN)_4]$ and V^{II}, Fe^{II}, Cr^{II}, and Cu^{I} ions under nonaqueous conditions lead to materials of unresolved composition and structure. IR spectra show multiple ν_{CN} bands ranging from ∼2050 to 2220 cm^{-1} indicating multiple phases, i.e., materials that possess a distribution of square planar and tetrahedral metal coordination geometries as well as CN linkage isomers.

Conclusion

Photochemical and thermal decomposition of $[PPN]_2[Mn^{IV}(CN)_6]$ leads to several characterized products, namely, $[PPN]_2[Mn^{II}(CN)_4]$ (**1**), $[PPN]_2[C_{12}N_{12}]$ (**2**), and $[PPN][C_4N_4]$ (**3**), as well as several uncharacterized products. This is the only route found thus far to synthesize $[Mn^{II}(CN)_4]^{2-}$ as direct combination of Mn^{II} salts and CN^- in nonaqueous media do not form this complex. Photochemical decomposition of $[Mn^{IV}(CN)_6]^{2-}$ in MeCN or CH_2Cl_2 is induced by a LMCT absorption whereas thermolysis of $[Mn^{IV}(CN)_6]^{2-}$ is a clean, quantitative route to $[Mn^{II}(CN)_4]^{2-}$. By either method, the end result is a two-electron reduction of Mn^{IV} with homolytic cleavage of two cyanide radicals. Only in CH_2Cl_2 are the conditions suitable for the formation of $[C_{12}N_{12}]^{2-}$ (**2**) in the time period of photolysis, and it is presumably formed by recombination and oligomerization of $CN^{\bullet}$ and CN^-. Longer periods of time and more dilute solutions lead to the isolation of $[C_4N_4]^-$ (**3**), and other $[CN]_x^{z-}$ species are also expected to be present. These results show that many unusual products can be formed as a consequence of C−C and C−N bond formation via the reaction of cyanogen and CN^- mediated by the presence of a cyanide-labile transition metal ion.

$[Mn^{II}(CN)_4]^{2-}$ is a building block for the preparation of four-coordinate extended network structures. Several new materials have been synthesized by nonaqueous routes and show that a wide variety of products are possible due to the lability of the $[Mn^{II}(CN)_4]^{2-}$ ion in solution. α-$Mn^{II}[Mn^{II}(CN)_4]$ is an interpenetrating sphalerite-type network structure with tetrahedral Mn centers and orders as an antiferromagnet below 65 K. β-$Mn^{II}[Mn^{II}(CN)_4]$ appears to be a disordered noninterpenetrating network structure with tetrahedral $[Mn^{II}(CN)_4]^{2-}$ centers and no long-range magnetic ordering above 2 K. When M^{II} cations besides Mn are reacted with $[Mn^{II}(CN)_4]^{2-}$, there is either cyanide abstraction or linkage isomerization due to the lability of tetracyanomanganate(II). α-$Mn^{II}[Co^{II}(CN)_4]$ is a disordered network structure with square planar $[Co^{II}(CN)_4]^{2-}$ that is thermally isomerized to a β-phase in the solid state, at elevated temperatures. The β-$Mn^{II}[Co^{II}(CN)_4]$ has tetrahedral Co^{II} and the same IR ν_{CN} absorption band as β-$Mn^{II}[Mn^{II}(CN)_4]$. $Mn^{II}[Ni^{II}(CN)_4]$ is stable as a disordered network solid with square planar Ni centers. The lack of other products attests to the stability of $[Ni^{II}(CN)_4]^{2-}$. In each of these materials there is antiferromagnetic coupling between nearest neighbor ions except for $Mn^{II}[Ni^{II}(CN)_4]$ that requires coupling of Mn ions through the diamagnetic $[Ni^{II}(CN)_4]^{2-}$ bridge.

Acknowledgment. The authors appreciate the determination of the structure of $[PPN][C_4N_4]$ by M. J. Scott and S. J. Lippard (MIT) and the constructive comments and insight provided by Prof. E. Coronado (Universidad de Valencia), Prof. A. J. Epstein, Dr. C. M. Wynn, and Mr. M. Girtu (The Ohio State University) and gratefully acknowledge the support from the DOE DMS

(Grant No. DE FG 03-93ER45504) and the American Chemical Society PRF (Grant No. 30722-AC5).

Supporting Information Available: An ORTEP atom-labeling diagram for [PPN][C_4N_4], [PPN]**3**. A summary of the crystallographic data, tables of fractional coordinates and isotropic thermal parameters, anisotropic thermal parameters, bond distances and angles, and hydrogen atom positions nonbonding distances for [PPN]**3** in CIF format. This material is available free of charge via the Internet at http://pubs.acs.org.

IC0012726